To be submitted to JPL Doc Rev for CS13

Comparison of Wavelength Dependent Giant Star Angular Diameters with Models

Gerard T. van Belle[1]

Michelson Science Center, California Institute of Technology, Pasadena, CA
gerard@ipac.caltech.edu

David R. Ciardi

Michelson Science Center, California Institute of Technology, Pasadena, CA
ciardi@ipac.caltech.edu

Peter Hauschildt

Hamburger Sternwarte, Universität Hamburg, Hamburg, Germany
peter.hauschildt@hs.uni-hamburg.de

and

Michael Scholz

Institut für Theoretische Astrophysik, Universität Heidelberg, Heidelberg, Germany; and
School of Physics, University of Sydney, Sydney, Australia
scholz@ita.uni-heidelberg.de

ABSTRACT

We present angular size measurements obtained with the Palomar Testbed Interferometer (PTI). Our sample includes 82 giant stars, with spectral types between B7 and M7. These objects represent the 'well studied' subset of giant stars observed at PTI (≥ 2 nights of observing per star, with an average of 17 samples per star). These objects have been rigorously vetted for binarity against the Hipparcos and FK6 catalogs. The PTI observations present 'narrowband' angular sizes in 0.1 μm increments across the K band, from 1.95 to 2.45 μm, with narrowband channel centers located at 2.0, 2.1, 2.2, 2.3, and 2.4 μm. There is strong evidence with later spectral types for a systematic increase in their 2.4 μm sizes relative to the 2.2 μm near-continuum center pixel, with weaker evidence for a similar effect in the 2.3 μm channel. There is little if any evidence for similar size differences between the 2.0 and 2.1 μm channels, relative to the band center. By comparing this data to publicly available near-IR spectrophometric data for stars of similar spectral type, there is a clear correlation between the strength of spectral features, including the ^{12}CO and ^{13}CO bands that set in longwards of 2.29μm, and the narrowband angular size differences. Giant star atmospheric models corresponding to the PTI 'narrowband' visibility data were generated from the extended model photospheres found in Bessel et al. (1989, 1991). For both the models and the observations, size ratios between the outlying wavelength pixels

[1]For preprints, please contact: gerard@ipac.caltech.edu.

relative to the 2.2 μm center pixel may be generated, along with effective temperature (T_{EFF}) estimates, and then compared. We find that for the stars with T_{EFF} between 3000K and 4000K, the observed 2.4μm / 2.2μm size ratios are significantly higher than predicted by the models.

Subject headings: infrared: stars, stars: fundamental parameters, techniques:interferometric

1. Introduction

One of the primary rationales for obtaining high-resolution observations of stellar targets is to test, constrain, and guide development of astrophysical models. Sufficiently detailed observations of stellar surface structure can not only characterize that surface but the underlying structure as well. An early example of this was the solar limb darkening observations of Pierce & Waddell (1961), from which the subsurface solar structure was constrained.

High-resolution observations of giant stars with near-infrared interferometers has the potential to extend to a large sample of stars a similar approach of comparisons of models to observational data. Due to a particular confluence of sensitivity and angular resolution, the current generation of interferometers is well suited to observe giant star diameters. Fortunately, it is for the coolest stars that models are least well constrained, which typify these luminosity class objects.

Some of the first models used extensively in comparison with interferometric data have been the models of Scholz & Takeda (1987), as seen in Richichi & Lisi (1990) and Benson et al. (1991), and as further developed in Bessell et al. (1989, 1991). More recent models developed by Hauschildt et al. (1999) also provide the apparent center-to-limb surface intensity variations necessary for comparison to observed interferometric visibility data.

In this second paper of the series concerning PTI observations of evolved stars, we report on comparisons of giant star angular diameters to predictions of stellar models. In ensuing manuscripts, we will detail PTI's observations of supergiants stars and carbon stars.

2. Observations

2.1. The Palomar Testbed Interferometer

PTI is a three-aperture interferometer located at Palomar Observatory in San Diego County, CA. Two of the 40 cm apertures may be used in conjunction for any single interferometric observation. The north and south piers used in this investigation are 109m apart on a baseline $\sim 20^o$ east of true north; the west pier in conjunction with the north provides an 85m baseline $\sim 70^o$ east of true north. Light from the two telescopes being linked interferometrically is reflected by transport optics into a central beam combining laboratory, where two delay lines are located. One of the two delay lines operates as a 'move-and-hold' element in the beam train for one of the telescopes, while the second moves dynamically during an observation with a precision of 10-20 nm. Following the delay line elements, the starlight is directed onto a beam combination table, where a dichroic splits off the visible light for tip-tilt sensing using a quad cell incorporating 4 fiber-fed avalanche photodiodes. After the dichroic, the two telescope beams are combined at a beam splitter. One of the two outputs from the beam splitter is fed directly into a dewar onto a single pixel of a NICMOS3 detector; this signal is referred to as the 'white-light channel'. The other output is fed through a single-mode

fiber and a prism outside the dewar, then onto five pixels on the detector chip; this signal constitutes the 'spectrometer channels'. Effective integration time for each pixel is ~6.75 ms. The white-light channel is utilized for fringe tracking in a manner similar to that use at the Mark III interferometer as described in Shao et al. (1988).

The channels used for visibility amplitude measurements reported herein are the spectrometer channels, which range in five 0.1 μm bins across the K band centered at 2.00, 2.10, 2.20, 2.30, and 2.40 μm. These channels, having been spatially filtered by a single-mode fiber before detection, were considerably less noisy than the white-light channel. To synthesize a "white light" result from the spectrometer channels, the results from the 5 narrowband pixels were averaged, resulting in an effective white-light K band measurement of $\lambda = 2.19 \pm 0.01\mu$m. For a more complete description of the instrument or the data reduction techniques, see Colavita (1999) or van Belle et al. (1999).

2.2. Interferometric Data

The interferometric observable used for these measurements is the fringe contrast or visibility (squared) of an observed brightness distribution on the sky. Normalized in the interval [0 : 1], a single star exhibits monochromatic visibility modulus in a uniform disk model given by

$$V^2 = \left[\frac{2J_1(\theta_{UD}\pi B\lambda^{-1})}{\theta_{UD}\pi B\lambda^{-1}}\right]^2, \tag{1}$$

where J_1 is the first-order Bessel function, B is the projected baseline vector magnitude at the star position, θ_{UD} is the apparent angular diameter of the star, and λ is the wavelength of the interferometric observation. The V^2 observables used in our Altair study are the synthetic wideband V^2's, given by an incoherent signal-to-noise (SNR) weighted average V^2 of the 5 narrowband channels in the PTI spectrometer (Colavita 1999). In a similar fashion, incoherent SNR-weighted average bandpasses λ were determined from the raw data. The PTI H and K wavebands are excellent matches to the CIT photometric system (Colavita et al. 1999; Elias et al. 1982, 1983). Separate calibrations and fits to the narrowband and synthetic wideband V^2 data sets yield statistically consistent results, with the synthetic wideband data exhibiting superior SNR. Consequently, we will present only the results from the synthetic wideband data.

Observations were carried out between September of 1997 and October of 2002. Each of the giant star targets, along with calibration objects, was observed multiple times during each of these nights, and each observation, or scan, was approximately 130 s long; an average of 250 scans were taken per month during the observing program. For each scan we computed a mean V^2-value from the scan data, and the error in the V^2 estimate from the rms internal scatter (Colavita 1999). Giant stars were always observed in combination with one or two calibration sources within 10° on the sky. The calibrator stars are expected to be nearly unresolved by the interferometer with predicted angular sizes typically less than 0.85 mas (86% were predicted to be less than 0.72 mas in size) ; expected angular size and error were based upon a blackbody radiator angular size inferred from available broadband photometry, particularly in the near-infrared (Gezari et al. 1996). Clearly, many stars deviate significantly from blackbody behavior (van Belle et al. 1999); however, the main sequence stars of F and G spectral type selected as primary calibrators should not deviate sharply from blackbody behavior. Table 1 identifies the calibrators, along with their V band magnitudes, spectral types and size estimates used in this study.

Table 1. Calibration sources for the observations.

Star	HIP	V (mag)	K (mag)	Spectral Type	$\theta_{\rm Estimate}$ (mas)
HD 2454	2235	6.05	4.94	F6Vawvar	0.44 ± 0.07
HD 6920	5493	5.67	4.46	F8V	0.56 ± 0.14
HD 7034	5544	5.15	4.39	F0V	0.53 ± 0.28
HD 7189	5677	7.07	4.80	G6III	0.54 ± 0.21
HD 7299	5717	6.74	4.43	G8III-IV	0.64 ± 0.23
HD 7476	5833	5.70	4.55	F5V	0.50 ± 0.14
HD 7804	6061	5.13	4.92	A3V	0.38 ± 0.12
HD 7964	6193	4.74	4.54	A3V	0.45 ± 0.18
HD 8272	6486	6.36	5.30	F4V	0.36 ± 0.06
HD 8723	6706	5.35	4.35	F2V:var	0.52 ± 0.14
HD 10497	8066	6.76	5.45	A7II	0.29 ± 0.03
HD 11151	8598	5.96	4.90	F5V	0.44 ± 0.10
HD 11973	9153	4.79	4.35	F0V	0.61 ± 0.24
HD 13555	10306	5.23	4.12	F5V	0.57 ± 0.18
HD 14055	10670	4.03	3.96	A1Vnn	0.58 ± 0.15
HD 17573	13209	3.61	3.86	B8Vn	0.55 ± 0.18
HD 18411	13879	4.68	4.42	A2Vn	0.44 ± 0.19
HD 20150	15110	4.87	4.83	A1V	0.39 ± 0.15
HD 23302	17499	3.72	3.92	B6III	0.33 ± 0.10
HD 23338	17531	4.30	4.50	B6V	0.31 ± 0.05
HD 24760	18532	2.90	3.71	B0.5V	0.34 ± 0.07
HD 25867	19205	5.21	4.29	F1V	0.54 ± 0.12
HD 27397	20219	5.58	4.85	F3V...	0.43 ± 0.10
HD 27459	20261	5.26	4.69	F0V	0.46 ± 0.16
HD 27819	20542	4.80	4.41	A7V	0.50 ± 0.15
HD 28024	20711	4.28	3.76	A8Vn	0.71 ± 0.15
HD 28052	20713	4.48	4.03	F0V...	0.71 ± 0.26
HD 28355	20901	5.02	4.53	A7V	0.46 ± 0.11
HD 29388	21589	4.27	4.11	A6V	0.61 ± 0.23
HD 30739	22509	4.35	4.17	A1Vn	0.51 ± 0.13
HD 31295	22845	4.64	4.42	A0V	0.41 ± 0.09
HD 31913	23360	7.51	5.26	G0IV	0.43 ± 0.05
HD 32630	23767	3.18	3.86	B3V	0.38 ± 0.06
HD 36576	26064	5.67	4.78	B2IV-Ve	0.19 ± 0.06
HD 37147	26382	5.53	4.94	F0V	0.45 ± 0.13
HD 37329	26571	6.45	4.18	G9III	0.80 ± 0.13
HD 38558	27338	5.47	4.48	F0III	0.57 ± 0.25
HD 41753	29038	4.42	4.85	B3IV	0.23 ± 0.05
HD 42560	29426	4.45	4.90	B3IV	0.22 ± 0.05
HD 42807	29525	6.43	4.85	G8V	0.46 ± 0.05
HD 43042	29650	5.20	4.13	F6V	0.67 ± 0.15
HD 43043	29637	6.66	4.45	G8III	0.70 ± 0.15
HD 45412	30827	5.75	3.92	F5.5Ibv	0.78 ± 0.19
HD 46300	31216	4.47	4.30	A0Ib	0.45 ± 0.13
HD 48682	32480	5.24	4.13	G0V	0.72 ± 0.17
HD 48805	32431	6.51	4.32	G8V	0.60 ± 0.26
HD 50019	33018	3.60	3.16	A3III	0.70 ± 0.12
HD 50692	33277	5.74	4.29	G0V	0.59 ± 0.12
HD 51530	33595	6.20	4.82	F8Vbwvar	0.45 ± 0.08
HD 52711	34017	5.93	4.54	G4V	0.58 ± 0.08
HD 56537	35350	3.58	3.54	A3V...	0.77 ± 0.21
HD 57006	35509	5.91	4.66	F8V	0.51 ± 0.11
HD 58715	36188	2.89	3.10	B8Vvar	0.75 ± 0.20
HD 58946	36366	4.16	2.98	F0V...	0.88 ± 0.09

Table 1—Continued

Star	HIP	V (mag)	K (mag)	Spectral Type	$\theta_{Estimate}$ (mas)
HD 59037	36393	5.07	4.74	A4V	0.41 ± 0.15
HD 60111	36723	5.59	4.83	F2V	0.45 ± 0.20
HD 69897	40843	5.13	3.87	F6V	0.69 ± 0.05
HD 79096	45170	6.49	4.66	G9V	0.55 ± 0.03
HD 79452	45412	5.98	3.86	G6III	0.87 ± 0.07
HD 79969	45617	7.20	4.77	K3V	0.54 ± 0.12
HD 81192	46155	6.53	4.12	G7III	0.72 ± 0.13
HD 82106	46580	7.20	4.79	K3V	0.53 ± 0.08
HD 82885	47080	5.40	3.69	G8IV-V	0.75 ± 0.09
HD 83362	47291	6.74	4.60	G8III	0.59 ± 0.25
HD 86728	49081	5.37	3.82	G1V	0.75 ± 0.07
HD 87696	49593	4.49	4.00	A7V	0.59 ± 0.09
HD 88737	50174	6.02	4.70	F9V	0.50 ± 0.11
HD 89125	50384	5.81	4.51	F8Vw	0.54 ± 0.06
HD 90125	50939	6.33	4.15	G9V	0.66 ± 0.18
HD 90277	51056	4.72	3.97	F0V	0.64 ± 0.23
HD 95128	53721	5.03	3.75	G0V	0.84 ± 0.07
HD 95382	53824	4.98	4.61	A5III	0.34 ± 0.08
HD 98824	55533	7.03	4.59	K1III	0.70 ± 0.17
HD 99984	56148	5.94	4.59	F4V	0.47 ± 0.08
HD 100655	56508	6.45	4.13	G9III	0.73 ± 0.24
HD 102634	57629	6.15	4.92	F7V	0.44 ± 0.09
HD 104556	58708	6.64	4.42	G8Vw...	0.53 ± 0.17
HD 109217	61246	6.29	4.27	G8III	0.74 ± 0.26
HD 110411	61960	4.88	4.68	A0V	0.36 ± 0.08
HD 110897	62207	5.95	4.47	G0V	0.55 ± 0.10
HD 115383	64792	5.19	4.03	G0Vs	0.75 ± 0.13
HD 118232	66234	4.68	4.27	A5V	0.51 ± 0.16
HD 121107	67787	5.71	4.08	G5III	0.68 ± 0.08
HD 121560	68030	6.16	4.84	F6V	0.44 ± 0.06
HD 122408	68520	4.23	4.09	A3V	0.41 ± 0.05
HD 127334	70873	6.36	4.74	G5V	0.51 ± 0.05
HD 128167	71284	4.47	3.34	F3Vwvar	0.82 ± 0.11
HD 130948	72567	5.86	4.46	G2V	0.55 ± 0.13
HD 133002	72573	5.63	3.92	F9V	0.63 ± 0.17
HD 134083	73996	4.93	3.86	F5V	0.70 ± 0.07
HD 137510	75535	6.26	4.84	G0V	0.48 ± 0.05
HD 141003	77233	3.65	3.55	A3V	0.74 ± 0.15
HD 144579	78775	6.66	4.76	G8V	0.50 ± 0.08
HD 145457	79219	6.57	4.12	K0III	0.74 ± 0.20
HD 145675	79248	6.61	4.71	K0V	0.55 ± 0.06
HD 152598	82587	5.34	4.56	F0V	0.51 ± 0.12
HD 154345	83389	6.76	5.00	G8V	0.47 ± 0.03
HD 157214	84862	5.38	3.91	G0V	0.71 ± 0.06
HD 157728	85157	5.70	5.18	F0IV	0.37 ± 0.17
HD 159222	85810	6.52	5.00	G5V	0.46 ± 0.03
HD 159332	85912	5.65	4.37	F6V	0.54 ± 0.06
HD 161868	87108	3.75	3.62	A0V	0.64 ± 0.08
HD 163641	87866	6.28	6.17	B9III	0.13 ± 0.06
HD 164259	88175	4.62	3.64	F3V	0.77 ± 0.04
HD 164353	88192	3.93	4.00	B5Ib	0.45 ± 0.12
HD 164595	88194	7.07	5.48	G2V	0.35 ± 0.04
HD 165195	88527	7.31	4.14	K3p	0.63 ± 0.29
HD 166205	85822	4.35	4.26	A1Vn	0.49 ± 0.16

The calibration of giant star V^2 data is performed by estimating the interferometer system visibility (V^2_{sys}) using calibration sources with model angular diameters and then normalizing the raw giant star visibility by V^2_{sys} to estimate the V^2 measured by an ideal interferometer at that epoch (Mozurkewich et al. 1991; Boden et al. 1998). Uncertainties in the system visibility and the calibrated target visibility are inferred from internal scatter among the data in a scan and standard error-propagation calculations. More detail on PTI's target & calibrator selection, data reduction (van Belle et al. 1999) and technical aspects (Colavita et al. 1999) is available in the literature. Calibrating our giant star data set with respect to the calibration objects listed in Table 1 results in a total of 2,117 calibrated scans on 116 giant stars over 766 nights between 1997 and 2002. Our calibrated narrowband V^2 measurements are summarized in Table 2, along with the stellar spectral type as listed in Table 3.

Table 1—Continued

Star	HIP	V (mag)	K (mag)	Spectral Type	$\theta_{\rm Estimate}$ (mas)
HD 173920	91985	6.26	4.38	G5III	0.73 ± 0.28
HD 178359	93990	7.09	4.21	F5IV	0.73 ± 0.06
HD 181440	95073	5.46	5.46	B9III	0.18 ± 0.06
HD 182900	95572	5.76	4.62	F6III	0.57 ± 0.20
HD 184006	95853	3.76	3.60	A5Vn	0.74 ± 0.27
HD 184606	96275	5.00	5.16	B8IIIn	0.18 ± 0.05
HD 184663	96351	6.37	5.36	F6IV	0.36 ± 0.10
HD 187923	97767	6.16	4.58	G0V	0.50 ± 0.10
HD 192425	99742	4.94	4.77	A2V	0.40 ± 0.11
HD 192640	99770	4.93	4.42	A2V	0.41 ± 0.08
HD 192985	99889	5.87	4.80	F5V:	0.46 ± 0.06
HD 193556	100274	6.17	4.25	G8III	0.81 ± 0.26
HD 195050	100907	5.63	5.41	A3V	0.31 ± 0.11
HD 196134	101467	6.50	4.10	K0III-IV	0.78 ± 0.16
HD 196180	101589	4.64	4.36	A3V	0.46 ± 0.17
HD 196360	101588	6.63	4.43	K0III	0.70 ± 0.25
HD 197076	102040	6.43	4.92	G5V	0.48 ± 0.06
HD 198726	102949	5.66	4.29	F5Ib	0.56 ± 0.21
HD 199081	103089	4.80	5.10	B5V	0.23 ± 0.06
HD 200723	103963	6.34	5.36	F3IV	0.36 ± 0.10
HD 201078	104185	5.77	4.37	F7.5Ib-IIv	0.63 ± 0.20
HD 201935	104592	6.69	5.39	F0III	0.27 ± 0.04
HD 204153	105769	5.59	4.74	F0V	0.45 ± 0.08
HD 206043	106897	5.77	4.96	F2V	0.42 ± 0.11
HD 206748	107198	7.57	5.16	G8Ib-II	0.53 ± 0.02
HD 207978	107975	5.52	4.33	F6IVwvar	0.57 ± 0.10
HD 210460	109439	6.18	4.47	G0V	0.50 ± 0.24
HD 210855	109572	5.24	3.98	F8V	0.67 ± 0.21
HD 211432	109977	6.38	4.11	G9III	0.76 ± 0.18
HD 211976	110341	6.18	5.05	F6V	0.42 ± 0.06
HD 212120	110351	4.55	4.77	B6V	0.28 ± 0.10
HD 212593	110609	4.55	4.28	B9Iab	0.45 ± 0.08
HD 213558	111169	3.76	3.85	A1V	0.61 ± 0.24
HD 214923	112029	3.41	3.57	B8.5V	0.62 ± 0.16
HD 216899	113296	8.68	4.52	M2:	0.74 ± 0.35
HD 217014	113357	5.45	3.91	G5V	0.71 ± 0.11
HD 217050	113327	5.34	5.24	B4IIIpe	0.18 ± 0.06
HD 218235	114081	6.16	5.07	F6Vs	0.42 ± 0.08
HD 218470	114210	5.68	4.65	F5V	0.50 ± 0.08
HD 218753	114365	5.68	4.62	A5III	0.59 ± 0.31
HD 218918	114520	5.15	4.74	A5Vn	0.41 ± 0.15
HD 219446	114835	7.79	5.27	G9III	0.47 ± 0.04
HD 220061	115250	4.58	4.09	A5V	0.54 ± 0.13
HD 220102	115228	6.62	4.84	F5II	0.54 ± 0.07
HD 221253	115990	4.89	5.16	B3IV	0.19 ± 0.02
HD 222173	116631	4.29	4.45	B8V	0.39 ± 0.24
HD 223421	117472	6.36	5.29	F2IV	0.36 ± 0.05

Table 2. Narrowband angular sizes of the observed giant stars.

Star	# Obs.	# Nights	$\theta_{2.2\mu m}$ (mas)	$r_{2.0\mu m}$	$r_{2.1\mu m}$	$r_{2.3\mu m}$	$r_{2.4\mu m}$
HD 6186	8	5	1.750 ± 0.044	0.953 ± 0.044	0.995 ± 0.030	0.976 ± 0.032	0.950 ± 0.039
HD 6409	11	5	1.865 ± 0.043	1.020 ± 0.030	1.014 ± 0.028	1.012 ± 0.029	1.023 ± 0.031
HD 7087	13	6	1.506 ± 0.045	1.046 ± 0.043	1.001 ± 0.033	1.009 ± 0.032	1.087 ± 0.044
HD 9927	10	6	3.466 ± 0.077	0.983 ± 0.006	0.990 ± 0.004	1.006 ± 0.005	1.022 ± 0.006
HD 10380	17	13	2.883 ± 0.053	1.007 ± 0.010	0.997 ± 0.009	1.000 ± 0.009	1.011 ± 0.011
HD 15656	9	3	2.464 ± 0.046	1.066 ± 0.018	1.009 ± 0.014	0.997 ± 0.015	1.007 ± 0.022
HD 17361	11	5	1.808 ± 0.043	1.003 ± 0.028	0.980 ± 0.019	1.005 ± 0.019	1.030 ± 0.026
HD 17709	13	6	3.747 ± 0.100	0.978 ± 0.003	0.993 ± 0.002	1.009 ± 0.003	1.022 ± 0.004
HD 23962	29	11	1.086 ± 0.055	0.995 ± 0.057	0.986 ± 0.042	0.989 ± 0.048	0.891 ± 0.068
HD 30605	12	3	1.821 ± 0.043	0.995 ± 0.029	1.014 ± 0.027	1.013 ± 0.025	1.039 ± 0.029
HD 35497	9	6	1.167 ± 0.113	1.133 ± 0.229	1.084 ± 0.144	1.129 ± 0.139	0.988 ± 0.235
HD 38656	11	9	1.524 ± 0.059	1.149 ± 0.101	1.195 ± 0.057	1.102 ± 0.054	1.206 ± 0.128
HD 40441	27	8	1.471 ± 0.045	1.103 ± 0.066	1.122 ± 0.036	1.084 ± 0.036	1.098 ± 0.105
HD 41467	6	4	0.992 ± 0.108	1.215 ± 0.247	1.088 ± 0.151	1.102 ± 0.150	1.600 ± 0.517
HD 46709	29	19	1.660 ± 0.044	1.033 ± 0.029	1.044 ± 0.023	1.003 ± 0.022	1.037 ± 0.029
HD 48450	15	14	1.971 ± 0.043	0.988 ± 0.023	0.983 ± 0.015	0.972 ± 0.015	1.020 ± 0.020
HD 49968	20	21	1.788 ± 0.044	1.005 ± 0.025	0.992 ± 0.018	0.979 ± 0.018	1.043 ± 0.023
HD 62721	33	15	2.831 ± 0.052	0.981 ± 0.008	0.997 ± 0.006	1.011 ± 0.006	1.017 ± 0.008
HD 73192	71	38	1.049 ± 0.056	1.014 ± 0.038	1.019 ± 0.033	1.002 ± 0.033	1.012 ± 0.040
HD 82381	8	3	2.132 ± 0.043	1.012 ± 0.045	0.970 ± 0.028	0.989 ± 0.030	1.113 ± 0.033
HD 87046	5	2	1.966 ± 0.043	0.824 ± 0.168	0.955 ± 0.033	0.976 ± 0.046	1.023 ± 0.070
HD 87837	16	4	3.213 ± 0.064	0.992 ± 0.011	0.985 ± 0.008	1.004 ± 0.008	1.052 ± 0.010
HD 90254	61	11	2.985 ± 0.056	0.988 ± 0.006	1.005 ± 0.005	1.010 ± 0.005	1.021 ± 0.005
HD 93287	4	2	1.592 ± 0.045	0.588 ± 0.369	0.924 ± 0.044	0.950 ± 0.065	0.970 ± 0.101
HD 94252	4	2	1.606 ± 0.072	0.749 ± 0.326	0.995 ± 0.073	0.943 ± 0.092	1.013 ± 0.140
HD 94264	10	5	2.491 ± 0.046	0.993 ± 0.008	1.004 ± 0.006	1.010 ± 0.006	1.023 ± 0.007
HD 95212	6	2	1.944 ± 0.056	1.064 ± 0.063	1.141 ± 0.043	1.057 ± 0.039	1.103 ± 0.050
HD 96833	3	3	3.805 ± 0.106	0.968 ± 0.003	0.990 ± 0.003	1.015 ± 0.003	1.022 ± 0.003
HD 104207	69	16	3.149 ± 0.062	0.989 ± 0.003	0.997 ± 0.002	1.015 ± 0.003	1.044 ± 0.003
HD 104575	6	3	1.697 ± 0.044	0.909 ± 0.097	0.944 ± 0.040	0.995 ± 0.045	0.996 ± 0.077
HD 104831	5	3	1.476 ± 0.063	0.906 ± 0.146	0.941 ± 0.066	1.010 ± 0.072	0.918 ± 0.127
HD 105943	8	2	1.758 ± 0.168	1.066 ± 0.146	1.010 ± 0.127	0.997 ± 0.145	0.901 ± 0.165
HD 107256	19	12	1.772 ± 0.044	0.990 ± 0.027	0.982 ± 0.018	1.005 ± 0.020	1.051 ± 0.023
HD 113226	10	5	3.079 ± 0.059	0.997 ± 0.006	0.995 ± 0.006	1.009 ± 0.006	1.029 ± 0.006
HD 114780	28	9	2.233 ± 0.043	1.004 ± 0.007	1.006 ± 0.006	1.005 ± 0.007	1.023 ± 0.007
HD 116207	23	10	2.119 ± 0.043	1.019 ± 0.011	1.006 ± 0.009	1.001 ± 0.010	1.021 ± 0.011
HD 118669	7	4	1.650 ± 0.044	1.012 ± 0.038	1.005 ± 0.035	1.010 ± 0.032	1.051 ± 0.036
HD 119584	3	2	1.366 ± 0.124	0.974 ± 0.155	1.060 ± 0.120	1.032 ± 0.130	1.061 ± 0.183
HD 121860	7	5	1.948 ± 0.043	1.013 ± 0.026	1.008 ± 0.023	1.022 ± 0.024	1.021 ± 0.025
HD 122316	2	2	3.786 ± 0.107	1.001 ± 0.005	0.997 ± 0.005	1.012 ± 0.004	1.060 ± 0.005
HD 123612	3	2	1.150 ± 0.142	0.912 ± 0.218	1.126 ± 0.162	1.057 ± 0.165	1.073 ± 0.258
HD 131111	48	6	1.186 ± 0.052	0.943 ± 0.025	0.977 ± 0.021	0.997 ± 0.021	1.016 ± 0.030
HD 133208	22	12	2.451 ± 0.045	0.995 ± 0.007	1.002 ± 0.006	1.005 ± 0.006	1.020 ± 0.007
HD 135722	27	11	2.682 ± 0.049	0.990 ± 0.005	0.998 ± 0.005	1.005 ± 0.005	1.016 ± 0.005
HD 137853	24	5	2.373 ± 0.044	1.012 ± 0.005	1.005 ± 0.005	1.015 ± 0.005	1.025 ± 0.006
HD 139971	14	6	1.668 ± 0.044	0.993 ± 0.028	1.030 ± 0.025	1.038 ± 0.025	1.099 ± 0.029
HD 147749	5	2	3.657 ± 0.090	0.978 ± 0.010	0.994 ± 0.008	1.002 ± 0.008	1.033 ± 0.011
HD 148897	24	7	1.932 ± 0.043	1.070 ± 0.021	1.061 ± 0.017	1.002 ± 0.016	1.006 ± 0.021
HD 150047	6	4	3.341 ± 0.071	0.980 ± 0.009	0.989 ± 0.007	1.003 ± 0.007	1.036 ± 0.009
HD 150997	16	9	2.426 ± 0.045	1.007 ± 0.009	1.002 ± 0.007	1.013 ± 0.007	1.019 ± 0.008
HD 152173	4	2	2.330 ± 0.054	1.088 ± 0.038	1.062 ± 0.033	0.977 ± 0.034	1.126 ± 0.040
HD 152326	7	5	1.691 ± 0.044	0.974 ± 0.043	0.983 ± 0.030	0.995 ± 0.032	1.022 ± 0.043
HD 153698	48	14	2.095 ± 0.043	1.009 ± 0.007	1.011 ± 0.006	1.017 ± 0.006	1.044 ± 0.007
HD 157617	81	40	1.261 ± 0.050	1.017 ± 0.022	0.999 ± 0.020	0.988 ± 0.020	1.014 ± 0.022

Table 2—Continued

Star	# Obs.	# Nights	$\theta_{2.2\mu m}$ (mas)	$r_{2.0\mu m}$	$r_{2.1\mu m}$	$r_{2.3\mu m}$	$r_{2.4\mu m}$
HD 163947	18	4	1.984 ± 0.043	1.005 ± 0.015	1.001 ± 0.012	1.003 ± 0.012	1.051 ± 0.017
HD 165683	3	2	1.082 ± 0.147	1.089 ± 0.187	1.010 ± 0.214	1.058 ± 0.188	1.121 ± 0.215
HD 166013	7	4	2.070 ± 0.044	1.025 ± 0.032	0.998 ± 0.023	1.012 ± 0.023	1.053 ± 0.025
HD 170137	50	29	1.795 ± 0.043	0.988 ± 0.015	1.000 ± 0.014	1.013 ± 0.014	1.040 ± 0.015
HD 173213	5	3	2.421 ± 0.045	0.975 ± 0.033	0.993 ± 0.021	1.006 ± 0.022	1.031 ± 0.026
HD 176670	15	5	2.310 ± 0.044	0.985 ± 0.014	0.996 ± 0.012	1.003 ± 0.013	1.031 ± 0.015
HD 180242	5	2	1.025 ± 0.132	0.993 ± 0.224	1.012 ± 0.179	1.065 ± 0.175	1.154 ± 0.250
HD 186675	62	20	1.307 ± 0.048	1.078 ± 0.032	1.007 ± 0.022	1.018 ± 0.022	1.029 ± 0.033
HD 193347	42	8	1.872 ± 0.043	1.008 ± 0.016	1.032 ± 0.011	1.015 ± 0.011	1.056 ± 0.016
HD 196643	11	8	1.222 ± 0.050	1.017 ± 0.085	1.008 ± 0.054	1.007 ± 0.052	1.042 ± 0.068
HD 197139	7	3	1.246 ± 0.071	0.941 ± 0.128	0.935 ± 0.074	1.010 ± 0.077	0.919 ± 0.126
HD 197912	12	34	1.982 ± 0.043	1.019 ± 0.021	0.998 ± 0.012	1.003 ± 0.016	0.998 ± 0.021
HD 198237	25	10	1.832 ± 0.043	1.015 ± 0.019	1.005 ± 0.015	1.043 ± 0.017	1.048 ± 0.024
HD 199697	26	5	1.976 ± 0.043	0.980 ± 0.017	0.989 ± 0.011	1.009 ± 0.011	1.049 ± 0.016
HD 205435	6	4	1.849 ± 0.043	1.021 ± 0.037	0.991 ± 0.029	0.987 ± 0.028	0.996 ± 0.032
HD 206749	3	2	3.039 ± 0.086	1.038 ± 0.078	1.139 ± 0.039	1.023 ± 0.037	1.096 ± 0.081
HD 214088	15	16	1.353 ± 0.056	0.857 ± 0.083	0.916 ± 0.054	0.956 ± 0.059	0.928 ± 0.075
HD 214245	7	3	1.121 ± 0.056	1.067 ± 0.078	0.992 ± 0.071	1.002 ± 0.071	1.072 ± 0.083
HD 214868	6	3	2.496 ± 0.046	0.995 ± 0.014	0.989 ± 0.011	0.999 ± 0.011	1.018 ± 0.015
HD 215665	16	8	2.170 ± 0.043	1.023 ± 0.011	0.991 ± 0.010	0.999 ± 0.010	1.003 ± 0.012
HD 216131	9	6	2.367 ± 0.044	1.001 ± 0.015	0.994 ± 0.011	1.003 ± 0.011	1.012 ± 0.016
HD 216174	4	21	1.468 ± 0.125	0.950 ± 0.211	0.947 ± 0.120	0.953 ± 0.108	0.918 ± 0.140
HD 218045	71	15	1.048 ± 0.056	0.990 ± 0.032	1.008 ± 0.027	1.017 ± 0.026	0.994 ± 0.038
HD 221345	6	4	1.329 ± 0.135	1.129 ± 0.208	1.190 ± 0.142	1.145 ± 0.133	0.964 ± 0.218
HD 221662	5	2	3.572 ± 0.087	1.009 ± 0.021	1.095 ± 0.011	1.018 ± 0.009	1.046 ± 0.026
HD 221905	4	2	2.295 ± 0.064	1.027 ± 0.090	1.036 ± 0.037	1.043 ± 0.035	1.116 ± 0.088
HD 223755	4	2	2.179 ± 0.071	1.059 ± 0.095	1.050 ± 0.043	1.045 ± 0.039	1.132 ± 0.097
HD 224303	3	2	2.131 ± 0.096	1.034 ± 0.115	1.157 ± 0.059	1.009 ± 0.057	1.025 ± 0.118

Table 3. Ancillary data for the observed giant stars.

Star	V (mag)	J (mag)	H (mag)	K (mag)	Spectral Type (lit.)	Ref.	Spectral Type
HD 6186	4.27	2.68	2.24	2.12	G9 IIIb Fe -2	KB99	G9
HD 6409	7.44	3.67	2.76	2.48	M2	G+93	M2
HD 7087	4.66	3.07	2.51	2.48	G8.5 III	KB99	G8.5
HD 9927	3.59	1.42	0.74	0.65	K3- III CN 0.5	KB99	K3
HD 10380	4.45	2.20	1.50	1.36	K3 III	KB99	K3
HD 15656	5.15	2.61	1.89	1.63	K5III	BSC	K5
HD 17361	4.52	2.88	2.35	2.10	K0.5 IIIb	KB99	K0.5
HD 17709	4.56	1.64	0.80	0.77	K5.5 III	KB99	K5.5
HD 23962	7.17	3.97	3.41	3.08	K5III	MP50	K5
HD 30605	6.09	3.40	2.54	2.40	gK3	BSC	K3
HD 35497	1.65	1.86	1.88	2.00	B7III	BSC	B7
HD 38656	4.51	2.90	2.44	2.25	G8 IIIb Fe -1	KB99	G8
HD 40441	6.69	3.61	2.85	2.45	K5III	F66	K5
HD 41467	6.15	4.12	3.55	3.30	K0III	BSC	K0
HD 46709	5.93	3.57	2.76	2.62	K4III	BSC	K4
HD 48450	5.42	2.63	1.90	1.70	K4III	BSC	K4
HD 49968	5.68	3.08	2.38	2.22	K5III	BSC	K5
HD 62721	4.89	2.07	1.28	1.24	K4 III	KB99	K4
HD 73192	5.96	4.44	3.71	3.62	gK2	BSC	K2
HD 82381	5.07	2.89	2.17	1.98	K2.5 III Fe -0.5	KB99	K2.5
HD 87046	7.36	3.26	2.46	2.19	M3III	this work*	M3
HD 87837	4.39	1.90	1.22	1.02	K3.5IIIbFe-1	BSC	K3.5
HD 90254	5.61	2.38	1.60	1.40	M3IIIabs	BSC	M3
HD 93287	8.23	4.25	3.38	2.95	M4III	this work	M4
HD 94252	7.37	4.12	3.10	2.93	M2III	R+97	M2
HD 94264	3.79	2.05	1.43	1.53	K0+ III-IV	KB99	K0
HD 95212	5.47	2.81	2.03	1.75	K5III	BSC	K5
HD 96833	3.00	1.03	0.38	0.43	K1 III	KB99	K1
HD 104207	6.94	2.68	1.67	1.46	M4III	Kwok+ 1997	M4
HD 104575	7.59	4.05	3.10	2.79	M3III	this work	M3
HD 104831	7.12	4.15	3.22	2.98	M1III	this work	M1
HD 105943	6.00	3.43	2.71	2.40	gK5	BSC	K5
HD 107256	8.25	3.69	2.76	2.42	M5III	L87	M5
HD 113226	2.85	1.25	0.73	0.66	G8 III-IIIb	KB99	G8
HD 114780	5.76	2.79	1.95	1.70	M0III	BSC	M0
HD 116207	7.59	3.52	2.63	2.28	M4III	this work	M4
HD 118669	7.55	3.51	2.66	2.33	M4III	this work	M4
HD 119584	6.12	3.94	3.17	2.81	K4III	BSC	K4
HD 121860	7.32	3.74	2.75	2.45	M4III	this work	M4
HD 122316	8.78	2.23	1.22	0.99	M8III	Kwok+ 1997	M8
HD 123612	6.57	4.08	3.28	3.09	K5III	H56	K5
HD 131111	5.47	3.64	3.11	2.88	K0III-IV	BSC	K0
HD 133208	3.49	1.80	1.27	1.22	G8IIIaBa0.3Fe-0.5	BSC	G8
HD 135722	3.46	1.66	0.99	1.22	G8III CN-1	MK73	G8
HD 137853	6.01	3.11	2.25	1.93	gM1	BSC	M1
HD 139971	7.68	3.52	2.69	2.37	M4III	this work*	M4
HD 147749	5.20	1.79	0.92	0.84	M2IIIab	BSC	M2
HD 150047	7.15	2.57	1.64	1.31	M6III	Kwok+ 1997	M6
HD 150997	3.48	1.77	1.37	1.33	G7.5IIIbFe-1	BSC	G7.5
HD 152173	5.73	2.89	2.07	1.85	M1IIIa	this work*	M1
HD 152326	5.03	3.11	2.56	2.36	K0.5IIIaCa0.5	BSC	K0.5
HD 153698	7.20	3.35	2.43	2.03	M4III	this work	M4
HD 157617	5.77	3.43	2.84	2.71	gK1	BSC	K1
HD 163947	8.42	3.40	2.42	2.19	M5III	this work	M5

3. Stellar Models

Examination of these narrowband measurements of stellar angular sizes are most useful in the context of stellar models. However, comparison of these sizes and the appropriate models presents a unique set of challenges. First, models appropriate to the narrowband observations must be generated. The uniqueness of the effective bandpasses of each PTI narrowband pixel dictates that models be specially generated for application to the PTI data. Second, the models and the observations need to be quantified in such a way as to permit direct intercomparison, allowing for the limitations of our current uniform disk data reductions. Third, the observed sizes must be properly normalized to intercompare the models and the observations.

Exploring this approach is useful in its potential to be expanded greatly for observations of significantly higher spectral resolution than are presented here. In order to test our approach, we will begin with the a well-established set of models first presented by Scholz and coworkers (Scholz & Takeda 1987; Bessell et al. 1989, 1991). These families of models are particularly useful here in that they are historically familiar to the near-infrared interferometry community, had center-to-limb surface brightness variations (CLVs) presented in their papers, and were readily adapable to generate model stellar atmospheres and their accompanying CLVs in the bandpasses specific to PTI to test the approach proposed here. These CLVs were generated for the A, U, X, and Z model families at the temperatures for which these models were available (2500, 2800, 3000, 3200, 3350, 3500, 3650, 3800K). Two of the CLV families for the PTI-specific bandpasses are plotted for the inspection of the reader: the Z350 model CLV family is shown in Figure 3, and the X250 model CLV family can be seen in Figure 2. The Z350 CLVs are all rather similar and indicative of a hotter, 3500K model; the X250 CLVs show substantial 'wings' in the 2.0 μm and 2.4 μm channels.

A more recent set of models has been developed by Hauschildt and coworkers, a grid of models collectively know the NextGen models (Hauschildt et al. 1999). These models cover a wide range of T_{EFF} and $\log(g)$ and describe both dwarf and giant stars. We selected a range of models corresponding to giant stars ranging in spectral type from G8 to M6, starting with values for T_{EFF} and R based upon the empirical measures given in van Belle et al. (1999). We then derived $\log(g)$ by using values for stellar mass that increased gradually from 1.1 $M_\odot$ to 1.2 $M_\odot$, indexed to spectral type as described in Allen (Cox 2000) (although we note that simply letting $M = 1.0 M_\odot$ for all stars does not alter our results in a significant manner). Once we had a range of T_{EFF} and $\log(g)$ values, selected the NextGen models that bracketed these values and interpolated our results below to match the spectral-type specific values for effective temperature and surface gravity.

Both the Scholz models and the NextGen models address the question of model giant star atmospheres in terms of spherical model atmospheres, which result in limb-darkening laws that depart significantly from one- or two-parameter characterizations (Orosz & Hauschildt 2000).

Once generated, a visibility curve for each the five narrowband CLVs from 2.0 to 2.4 μm for a given model was generated by the standard technique of Fourier transformation of a strip brightness profile generated from the CLV. For each of the five narrowband CLVs for an individual model, a visibility curve was then fit with a uniform disk visibility curve. For each of these five uniform disk fits, a gross size parameter resulted, and size ratios of the outlying narrowband sizes relative to the central 2.2μm pixel could then be generated. These ratios can then be compared to comparable the size ratios already obtained on the stars observed, as a function of the models' pre-determined effective temperature.

This approach has many inherent advantages:

- By using the narrowband size *ratios*, no normalization is necessary to compare the true physical sizes of the observed stars with the predicted linear sizes of the models. This is particularly useful in that

Table 3—Continued

Star	V (mag)	J (mag)	H (mag)	K (mag)	Spectral Type (lit.)	Ref.	Spectral Type
HD 166013	7.33	3.09	2.27	1.94	M4III	this work*	M4
HD 170137	6.07	3.48	2.74	2.41	M0III	BSC	M0
HD 173213	8.20	3.31	2.36	1.90	M5III	L87	M5
HD 176670	4.94	2.40	1.74	1.57	K2.5IIIBa0.5	BSC	K2.5
HD 186675	4.89	3.45	2.94	2.64	G7+III	BSC	G7.5
HD 193347	6.61	3.44	2.69	2.31	M2III	H56	M2
HD 196643	7.09	4.60	3.66	3.17	K5III	MP50	K5
HD 197139	5.97	4.26	3.49	3.27	K2III	BSC	K2
HD 197912	4.22	2.39	1.83	1.70	G9.5III	BSC	G9.5
HD 198237	6.41	3.58	2.76	2.35	K3III	BSC	K3
HD 199697	5.30	2.62	1.98	1.77	K3.5III	BSC	K3.5
HD 205435	3.98	2.49	2.01	1.90	G8III CN-1, Hydr. str.	MK73	G8
HD 206749	5.51	2.52	1.70	1.50	M2IIIab	BSC	M2
HD 214088	7.25	4.30	3.47	3.14	K5III:	B57	K5
HD 214245	7.06	4.55	3.70	3.58	K5III	MP50	K5
HD 214868	4.50	2.44	1.82	1.67	K2+III-IIIb	BSC	K2
HD 215665	3.97	2.03	1.46	1.51	G8IIIa*	BASK	G8
HD 216131	3.51	1.70	1.24	1.18	G8III+	MK73	G8
HD 216174	5.43	3.58	2.92	2.63	K1III	BSC	K1
HD 218045	2.49	2.54	2.74	2.65	B9III	K83	B9
HD 221345	5.22	3.02	2.61	2.33	K0III	BSC	K0
HD 221662	6.10	2.20	1.31	1.10	M3III	BSC	M3
HD 221905	6.44	2.96	2.11	1.78	M1III	BSC	M1
HD 223755	6.13	3.25	2.33	2.09	M2III	BSC	M2
HD 224303	6.18	2.97	2.16	1.96	M2III	BSC	M2

Note. — V magnitudes taken from Hipparcos (Perryman 1997); J, H, & K magnitudes from 2MASS (Cutri et al. 2003).

References. — B57, Bidelman (1957); BSC, Hoffliet & Warren (1991); F66, Fehrenbach (1966); H56, Heard (1956); K83, Kennedy (1983); KB99, Keenan & Barnbaum (1999); M56, Moore & Paddock (1950); MK73, Morgan & Keenan (1973)

it eliminates the need for knowledge of the distance to the observed stars.

- Using uniform disk visibility fits to the model CLVs does not properly fit the CLVs' visibility curves. However, for the central lobe of the visibility curve, which is indicative of the overall size structure in question, the fit is nearly exact (with a few percent). More importantly, the fitting of a uniform disk visibility curve to the model CLVs mimics exactly what has been done in the observational portion of this investigation, where a uniform disk visibility curve has been fit to the observed stellar visibility data. If the models precisely predict the true CLVs of the observed stars, than any subtle biases inherent in this imperfect fitting should not be evident when the theoretically and empirically established ratios are compared.

All of the concerns outlined at the beginning of this section are addressed by this approach. We expect that this approach is greatly extensible once higher spectral resolution interferometers are available, and will permit examination of particular radiating layers associated with certain spectral features in the context of sophisticated models.

The results of this approach are plotted for the four PTI ratios (2.0, 2.1, 2.3, 2.4 to 2.2 μm) in Figures 4-7. The lines fit to the observational data found in these Figures are:

$$\theta_{2.0\mu}/\theta_{2.2\mu} = 1.009 \pm 0.057 + T_{EFF} \times (-2.80 \pm 12.92) \times 10^{-6} \quad (2)$$

$$\theta_{2.1\mu}/\theta_{2.2\mu} = 1.009 \pm 0.052 + T_{EFF} \times (-2.80 \pm 11.72) \times 10^{-6} \quad (3)$$

$$\theta_{2.3\mu}/\theta_{2.2\mu} = 1.026 \pm 0.049 + T_{EFF} \times (-3.64 \pm 10.93) \times 10^{-6} \quad (4)$$

$$\theta_{2.4\mu}/\theta_{2.2\mu} = 1.090 \pm 0.061 + T_{EFF} \times (-14.12 \pm 13.71) \times 10^{-6} \quad (5)$$

As is evident in the figures, there is only a marginal amount of overlap between the effective temperatures of the observed stars and the models' effective temperatures. However, these plots allow us to investigate the match between the cool end of the observational ratio data and the various warmer models. The shorter wavelength 2.0 and 2.1 μm ratio plots appear to be in agreement with the simple expectation of unit ratios at 3500K of all the models. For the 2.3 μm ratio data, the observational data are beginning to indicate a ratio slightly larger than all of the models, although this is not statistically significant. However, this trend continues in a significant way with the 2.4 μm data see in Figure 7. At 3500K, the observed ratio is ~ 1.04, 2% higher than the value predicted by all of the models.

4. Acknowledgements

We acknowledge fruitful discussions with TBD. We would also like to thank the gracious Palomar Mountain staff and PTI Collaboration for their support of this observing program. Funding for PTI was provided to the Jet Propulsion Laboratory under its TOPS (Towards Other Planetary Systems), ASEPS (Astronomical Studies of Extrasolar Planetary Systems), and Origins programs and from the JPL Director's Discretionary Fund. Portions of this work were performed at the Jet Propulsion Laboratory, California Institute of Technology under contract with the National Aeronautics and Space Administration. This publication makes use of data products from the Two Micron All Sky Survey, which is a joint project of the University of Massachusetts and the Infrared Processing and Analysis Center/California Institute of Technology, funded by the National Aeronautics and Space Administration and the National Science Foundation. This research has made use of the SIMBAD database, operated at CDS, Strasbourg, France.

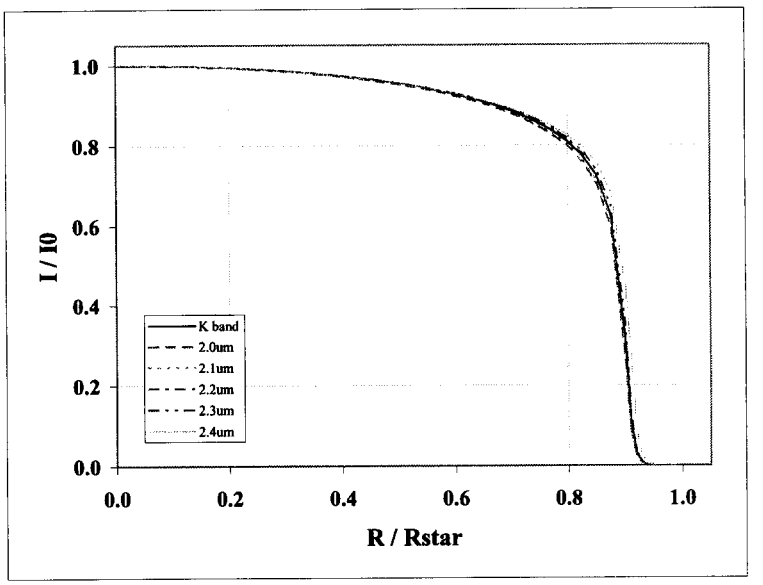

Fig. 1.— Center-to-limb variation (CLV) family from Bessell et al. (1989, 1991), from the Z350 model. Blah.

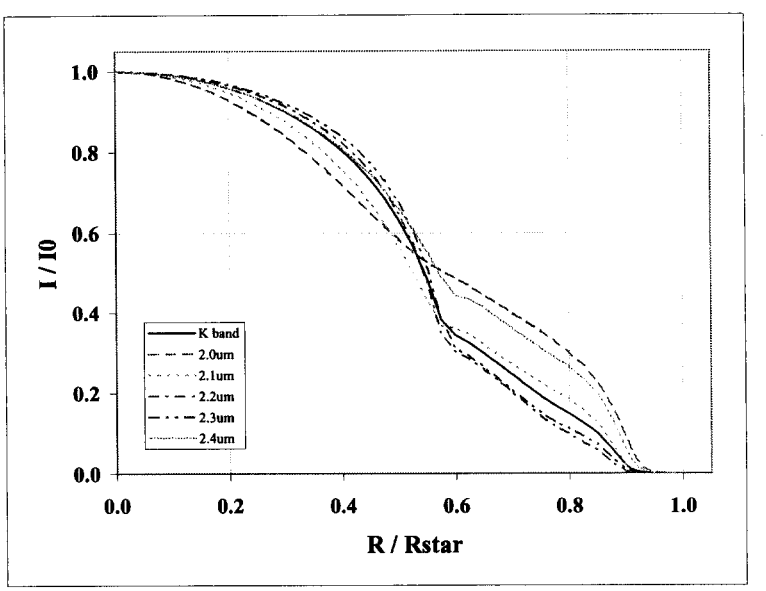

Fig. 2.— Center-to-limb variation (CLV) family from Bessell et al. (1989, 1991), from the X250 model. Note the substantial 'wings' at 2.0 & 2.4 μm for the cooler X250 model.

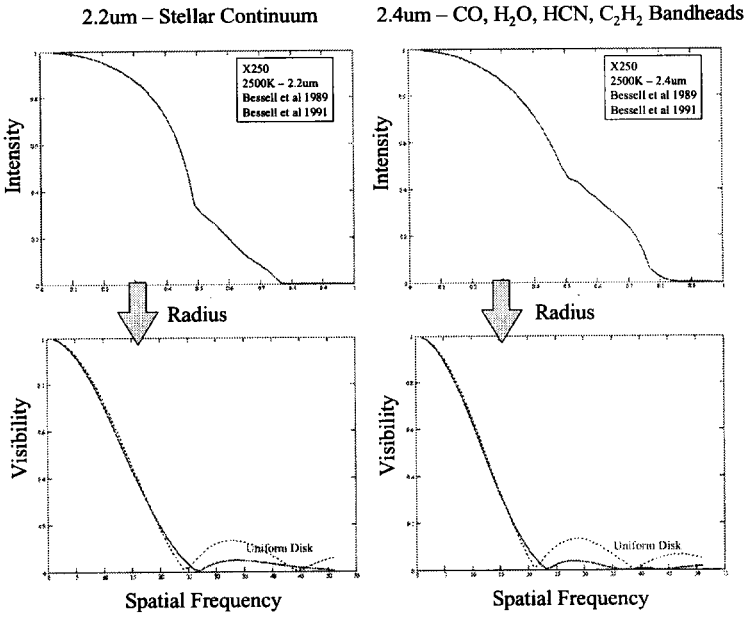

Fig. 3.— An example of CLVs for two separate bandpasses of the same model. The 2.2 μm continuum bandpass has weaker 'wings' than the 2.4 μm bandpass, and as such shows a UD fit that is indicative of a smaller star than that of the 2.4 μm channel.

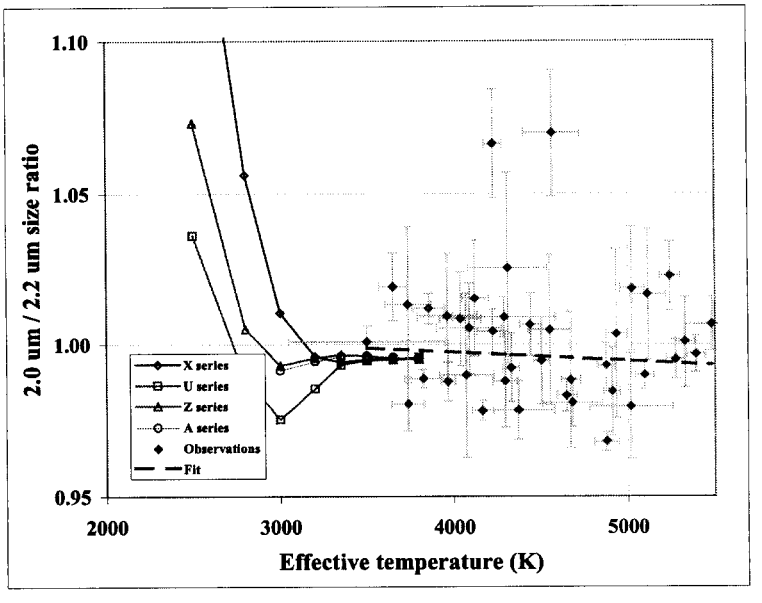

Fig. 4.— 2.0 μm to 2.2 μm.

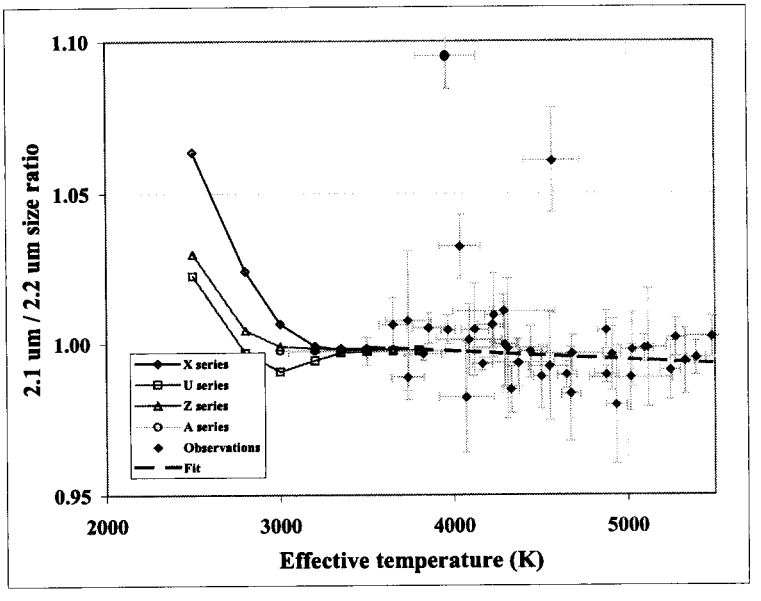

Fig. 5.— 2.1 μm to 2.2 μm.

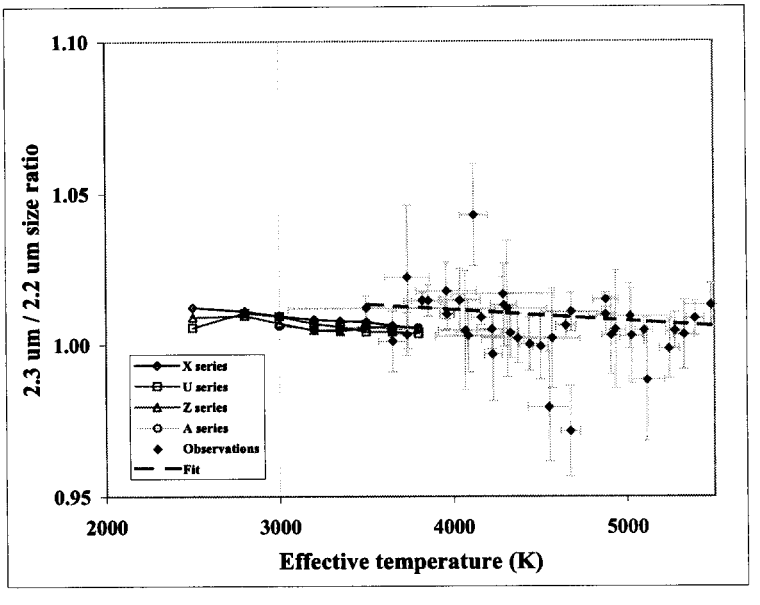

Fig. 6.— 2.3 μm to 2.2 μm.

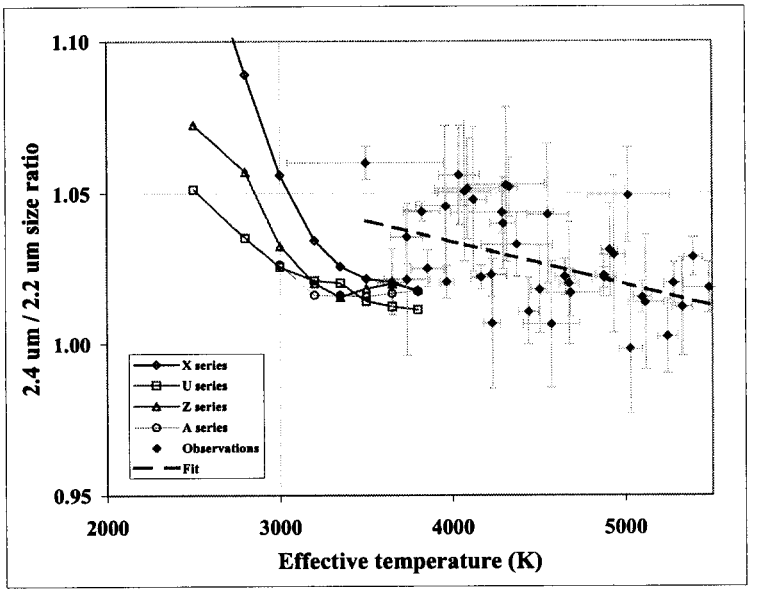

Fig. 7.— 2.4 μm to 2.2 μm.

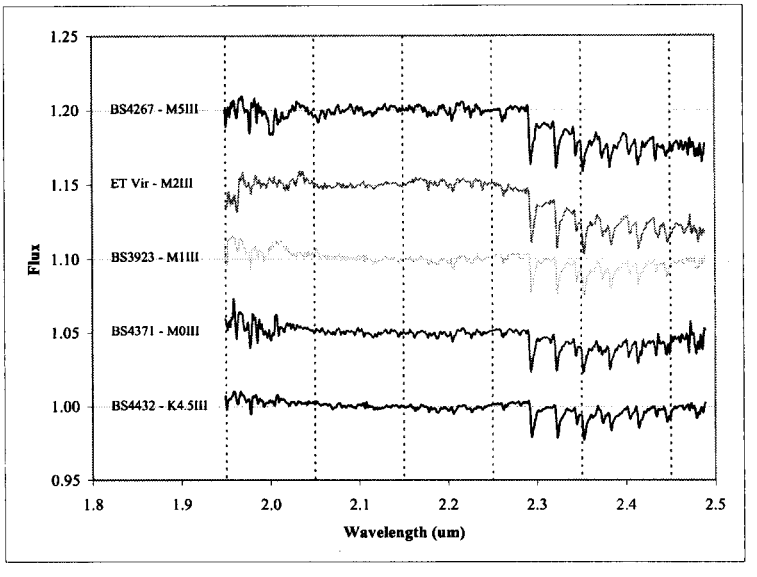

Fig. 8.— Sample giant star spectra taken from the atlas of Lançon & Wood (2000). The relative K band fluxes are shifted by 0.05 units to assist inspection. Of particular interest The vertical dotted lines represent the edges of the PTI spectral channels.

REFERENCES

Allen, C.W., 1973, Astrophysical Quantites, London: University of London, Athlone Press, 3rd ed

Alonso, A., Arribas, S., Martinez-Roger, C., 1994, A&A, 282, 684

Barnbaum, C., Morris, M., Kahane, C., 1995, ApJ, 450, 862

Baron, R.L., French, R.G., Elliot, J.L., 1989, Icarus 78, 119

Benson, J. A., Dyck, H. M., Mason, W. L., Howell, R. R., Ridgway, S. T., & Dixon, D. J. 1991, AJ, 102, 2091

Bessell, M. S., Brett, J. M., Scholz, M., & Wood, P. R. 1991, A&AS, 89, 335

Bessell, M. S., Brett, J. M., Wood, P. R., & Scholz, M. 1989, A&AS, 77, 1

Bidelman, W.P., 1957, PASP, 69, 326

Blackwell, D.E., Petford, A.D., Shallis, M.J., 1979, A&A, 82, 249

Boden, A.F, et al., 1998, ApJ, 504, L39

Brouwer, D., Clemence, G.M., 1961, in *The Solar System III*, eds. G.P. Kuiper, B.M. Middlehurst (Chicago:Univ. of Chicago Press), pp. 31-94

Carpenter, K.G., Slettebak, A., Sonneborn, G., 1984, ApJ, 286, 741

Claret, A., Diaz-Cordoves, J. & Gimenez, A., 1995, A&AS, 114, 247

Claret, A., 2000, A&A, 359, 289

Cohen, M., Walker, R.G., Carter, B., Hammersley, P., Kidger, M., Noguchi, K., 1999, AJ, 117, 1864

Colavita, M.M., 1999, PASP, 111, 111

Colavita, M.M., et al., 1999, ApJ, 510, 505

Cox, A. N. 2000, Allen's astrophysical quantities, 4th ed. Publisher: New York: AIP Press; Springer, 2000. Editedy by Arthur N. Cox. ISBN: 0387987460

Cutri, R. M. et al. 2003, VizieR Online Data Catalog, 2246, 0

de Medeiros, J.R., Mayor, M., 1999, A&AS 139, 433

Dyck, H. M., Benson, J. A., van Belle, G. T., Ridgway, S. T. 1996, AJ, 111, 1705

Dyck, H. M., van Belle, G. T., Thompson, R. R. 1998, AJ, 116, 981

Elias, J., Frogel, J., Hyland, A., Jones, T., 1983, AJ, 88, 1027

Elias, J., Frogel, J., Matthews, K., Neugebauer, G., 1982, AJ, 87, 1029

Elliot, J.L., Nicholson, P.D., 1984, in *Planetary Rings*, eds. R. Greenberg, A. Brahic, (Tucson:Univ. of Arizona Press), pp. 25-72

Fehrenbach, C., 1966, Publ. Obs. Haute-Provence, 8, 25

Freire Ferrero, R., Praderie, F., Czarny, J., Felenbok, P., 1978, A&A, 61, 785

Freire Ferrero, R., Gouttebroze, P., Catalano, S., Marilli, E., Bruhweiler, F., Kondo, Y., van der Hucht, K., Talavera, A., 1983, ApJ, 439, 1011

Gatewood, G., de Jonge, J.K., 1995, ApJ, 450, 364

Gezari, D.Y., Pitts, P.S., Schmitz, M., 1996, Catalog of Infrared Observations, edition 3.5

Gliese, W., Jahreiss, H., 1991, Preliminary Version of the third catalogue of nearby stars

Gouttebroze, P., Freire Ferrero, R., Marilli, E., Catalano, S., 1999, A&A, 348, 198

Gray, D.F., 1976, The Observation and Analysis of Stellar Photospheres, New York, Wiley-Interscience

Gulliver, A.F., Hill, G., Adelman, S.J., 1994, ApJ, 429, L81

Hauschildt, P. H., Allard, F., Ferguson, J., Baron, E., & Alexander, D. R. 1999, ApJ, 525, 871

Heard, J.F. 1956, Publ. David Dunlap Obs., 2, 105

Hoffleit, D., Warren, W.H. Jr., 1991, The Bright Star Catalog, Astronomical Data Center, NSSDC/ADC

Kahane, C., Maizels, C., Jura, M., 1988, ApJ, 328, L25

Keenan, P.C., Barnbaum, C., 1999, ApJ, 518, 859

Kennedy, P.M., 1983, MK Classification Catalogue Extension, Mt. Stromlo & Siding Spring Observatories, Australia

Kuchner, M.J., Brown, M.E., 2000, PASP, 112, 827

Hanbury Brown, R., Davis, J., Allen, L.R., Rome, J.M., 1967, MNRAS, 137, 393

Hanbury Brown, R., Davis, J., Allen, L.R, 1974, MNRAS, 167, 121

Haniff, C.A., Scholz, M., Tuthill, P.G., 1995, MNRAS, 276, 640

Hofmann, K.-H., Scholz, M., 1998, A&A, 335, 637

Johnson, H.L., Morgan, W.W., 1953, ApJ, 117, 313

Jordahl, P.R., 1972, Ph.D. thesis, University of Texas at Austin.

Lançon, A. & Rocca-Volmerange, B. 1992, A&AS, 96, 593

Lançon, A. & Wood, P. R. 2000, A&AS, 146, 217

Lattanzi, M.G., Munari, U., Whitelock, P.A., Feast, M.W., 1997, ApJ, 485, 328

Maeder, A., 1997, A&A, 321, 134

Maeder, A., 2000, New Astronomy Reviews, 44, 291

Malagnini, M.L., Morossi, C., 1990, A&AS, 85, 1015

Martin, E.L., Claret, A., 1996, A&A, 306, 408

Monnier, J.D., Tuthill, P.G., Danchi, W.C., 1999, ApJ, 525, L97

Moore, J.H., Paddock, G.F., 1950, ApJ, 112, 48

Morgan, W.W., Keenan, P.C., 1973, ARA&A, 11, 29

Mozurkewich, D., et al., 1991, AJ, 101, 2207

Mozurkewich, D., et al., 2003, AJ, in press

Nordgren, T.E., 2000, private communication

Nordgren, T.E., Sudol, J.J., Mozurkewich, D., 2001, AJ, 122, 2707

Nordgren, T.E., et al., 1999, AJ, 118, 3032

Nordgren, T.E., Dyck, H.M., 2002, AJ, 124, 541

Orosz, J. A. & Hauschildt, P. H. 2000, A&A, 364, 265

Perryman, M.A.C., et al., 1997, A&A, 323, 49

Pierce, A. K. & Waddell, J. H. 1961, MmRAS, 63, 89

Piirola, V., 1977, A&AS, 30, 213

Press, W.H., Teukolsky, S.A., Vetterling, W.T., Flannery, B.P., 1992, Numerical Receipes in C, Port Chester, Cambridge University Press

Richichi, A. & Lisi, F. 1990, A&A, 230, 355

Russell, J.L., Gatewood, G.D., Wagman, N.E., 1978, AJ, 83, 1455

Schlesinger, F., 1909, Publ. Allegheny Observatory, 1, 134

Schlesinger, F., 1911, MNRAS, 71, 719

Scholz, M., & Takeda, Y. 1987, A&A, 186, 200

Shallis, M.J., Blackwell, D.E., 1980, A&A, 81, 336

Shao, M., Colavita, M.M., Hines, B.E, Staelin, D.H., Hutter, D.J., 1988, A&A, 193, 357

Slettebak, A., 1949, ApJ, 110, 498

Slettebak, A., 1985, in Calibration of Fundamental Stellar Quantities, Dordrecht, D. Reidel Publishing Co., p. 163-184.

Stoeckley, T.R., 1968, MNRAS, 140, 121

Thompson, R.R., Creech-Eakman, M.J., van Belle, G.T., 2002, ApJ, 577, 447

Tinbergen, J., 1982, A&A, 105, 53

Tuthill, P.G., 1994, Ph.D. thesis, Univ. of Cambridge

van Belle, G.T., Dyck, H.M., Benson, J.A., Lacasse, M.G., 1996, AJ, 112, 2147

van Belle, G.T., Dyck, H.M., Thompson, R.R., Benson, J.A., Kannappan, S.J., 1997, AJ, 114, 2150

van Belle, G.T., Lane, B.F., Thompson, R.R., The PTI Collaboration, 1999, AJ, 117, 521

van Belle, G.T., Ciardi, D.R., Boden, A.F., Thompson, R.R., Creech-Eakman, M.J., submitted to ApJ

This preprint was prepared with the AAS LaTeX macros v5.2.